

# Origins of Chevron Rollovers in Non-Two-State Protein Folding

## Kinetics

Hüseyin KAYA and Hue Sun CHAN

*Protein Engineering Network of Centres of Excellence,*

*Department of Biochemistry, and*

*Department of Medical Genetics & Microbiology*

*Faculty of Medicine, University of Toronto*

*Toronto, Ontario M5S 1A8, Canada*

## Abstract

Chevron rollovers of some proteins imply that their logarithmic folding rates are nonlinear in native stability. This is predicted by lattice and continuum Gō models to arise from diminished accessibilities of the ground state from transiently populated compact conformations under strongly native conditions. Despite these models' native-centric interactions, the slowdown is due partly to kinetic trapping caused by some of the folding intermediates' non-native topologies. Notably, simple two-state folding kinetics of small single-domain proteins are not reproduced by common Gō-like schemes.

PACS Numbers: 87.15.Aa, 87.15.Cc, 87.15.He, 87.15.By

The physical basis of protein folding is a central unresolved puzzle in molecular biology. Recently, much advance in protein folding has originated from experiments on small single-domain proteins [1] with simple two-state folding and unfolding kinetics typified by that of CI2 [2], with features including: (i) single-exponential relaxation, (ii) the logarithmic folding and unfolding rates ( $\ln k_f$  and  $\ln k_u$ ) at constant temperature being essentially linear in chemical denaturant (urea or GuHCl) concentration, i.e., both arms of the “chevron plot” [3] are linear, and that (iii) the equilibrium ratio of native to denatured conformational population  $K \equiv [\text{native}]/[\text{denatured}] = k_f/k_u$ . What form of intrachain interactions might give rise to such remarkable behavior is a question of fundamental biophysical interest.

Other proteins’ corresponding properties are more complex. Often this is manifested by significant deviations [4–9] from the above linearities, i.e., they exhibit chevron rollovers [10]. We refer to their kinetics as non-two-state. Examples of such behavior include barnase [4,8], ribonuclease A [5], hen lysozyme [6], and U1A [7]. The present operational definition of non-two-state kinetics encompasses what some authors called “two-state” (though not “simple”) when conditions (i) and (iii) above are satisfied but not (ii) [7,8]. Chevron rollover can also be brought about by mutation, as in S6 [7] and BPTI [9]. Thus, rather than an aberration, chevron rollover is quite ubiquitous. Therefore, ascertaining its physical origins should provide important clues to protein energetics.

Chevron rollovers have been attributed to peculiarities of intermediates or transition states on postulated free energy profiles [4–8,10], or front factors’ sensitivity to folding conditions [11]. Yet these phenomenological considerations do not pinpoint the physical processes involved. In this Letter, physical mechanisms underlying chevron rollovers are addressed directly by examining a multitude of trajectories from several protein chain models.

The recent discovery of a remarkable correlation between contact order and folding rates of simple two-state proteins [12] has led to extensive studies of G $\bar{o}$ -like protein models [13–17]. Hence, a natural question is whether common G $\bar{o}$ -like constructs do predict simple two-state kinetics. Somewhat surprisingly, our investigation thus far indicates that this may not be the case. Instead, chevron rollover emerges as a conspicuous feature in both lattice

[11] and continuum [17]  $G\bar{o}$  models. This suggests that common native-centric [16] chain constructs can be useful for elucidating the polymer mechanisms of chevron rollovers, even though they may not be entirely adequate for simple two-state proteins. Pursuing this logic, we now analyze a thermodynamically cooperative [16] 48mer three-dimensional lattice  $G\bar{o}$  model [14]. This model had notable impact on recent appraisals [18] of the energy landscape views of protein folding [19], but its chevron behavior has not been investigated.

Each native contact in this model has a favorable energy  $\epsilon$  ( $< 0$ ), nonnative contacts have zero energy. Folding/unfolding kinetics are modeled by Metropolis Monte Carlo (MC) dynamics with the same set of elementary chain moves as in [14]: End moves are attempted for the two chain-end monomers. Corner and crankshaft moves are attempted for other monomers with 70% and 30% probability respectively. Time is measured by the number of attempted MC moves;  $Q$  is fractional number of native contacts [15,17].

The chevron plots for this  $G\bar{o}$  model and a closely related model are shown in Fig. 1. When relaxation is single-exponential (see below),  $k_f$  or  $k_u = 1/\text{MFPT}$ . Most of the MFPTs here are averaged from at least 1,000 trajectories, except for a narrow  $\epsilon/k_B T$  range around the transition midpoint where kinetics are relatively slow (100–200 trajectories each) and for folding initiated from Fig. 2(d) (200 trajectories each). In these models, the free energy  $\Delta G_u$  of unfolding to the open conformations ( $Q \leq 6/57$ ) is essentially linear in  $\epsilon/k_B T$ . Thus we model denaturant concentration changes by varying  $\epsilon/k_B T$  [11,20]. Adding repulsive nonnative contact energies to a  $G\bar{o}$  model [20,21] does not appear to have a significant impact on the chevron behavior. Fig. 1 shows dramatic chevron rollovers of the folding arms and very slight rollovers of the unfolding arms for both models, with maximum folding rates at  $\Delta G_u/k_B T = 14.2$  ( $G\bar{o}$ ) and 16.2 ( $G\bar{o}$  plus repulsion). Fig. 1 indicates that deviations from simple two-state behavior can be difficult to discern under weakly native conditions [22]. To facilitate comparison with experiments, we characterize folding rollover by the difference between the hypothetical simple two-state  $\ln k_f^{2-s}$  (inclined dotted lines in Fig. 1) and the actual (simulated) folding rate  $\ln k_f \approx -\ln(\text{MFPT})$  at three representative values of native stability  $\Delta G_u$ , spanning a range typically covered by real proteins. Here, for  $\Delta G_u/k_B T = (5,$

10, 15), the logarithmic rollover ratio  $\ln(k_f^{2-s}/k_f) = (0.16, 1.08, 2.96)$  for the Gō model and  $(0.32, 1.36, 3.12)$  for the model with repulsive interactions. These ratios are not dissimilar to the corresponding  $\ln(k_f^{2-s}/k_f) \approx (0.77, 2.42, 4.28)$  for wildtype barnase at 25°C and pH 6.3 [4]. Under these conditions, a maximum folding rate was not observed for barnase [4]. However, if a quadratic dependence [7,23] of  $\ln k_f$  vs. denaturant is assumed for barnase (c.f. [8]), a maximum folding rate  $\approx 230 \text{ s}^{-1}$  may be extrapolated to occur at an hypothetical  $\Delta G_u \approx 40k_B T$  which is much more stable than the  $\Delta G_u \approx 18.0k_B T$  at zero denaturant.

Fig. 2(a) provides the Gō model’s conformational distributions at different native stabilities. Under mildly native conditions ( $\Delta G_u < 10k_B T$ ), the free energy profiles have a barrier between the native and denatured minima. Under more strongly native conditions ( $\Delta G_u > 15k_B T$ ), their shapes are suggestive of downhill folding [24]. The analysis of first passage time distribution [16,25] in Fig. 2(b) indicates that folding kinetics is approximately single exponential [ $\ln P(t)$  linear in  $t$ ] under mildly native conditions, consistent with the observed single-exponential folding kinetics for ribonuclease A when double-jump experiments were used to eliminate the effect of *cis/trans* proline isomerization [5]. The behavior of wild-type barnase is similar: Folding is fast and single-exponential for the majority of the chains ( $\approx 80\%$ ), the rest belongs to a slow-folding tail caused by proline isomerization [4]. However, when modeling conditions are strongly native (corresponding conditions may not always be experimentally achievable [11]), folding kinetics is not single-exponential [circles and squares in Fig. 2(b)]. The onset of this behavior occurs approximately when the  $-\ln[P(Q)]$  profile becomes downhill and where folding rate is maximum (c.f. Figs. 1 and 2) [11]. It would be instructive to ascertain whether this specific model prediction applies to real proteins.

A closer examination of the model folding trajectories indicates that the slowdown leading to folding-arm chevron rollovers arises from transiently populated compact non-ground-state conformations because these folding “intermediates” have lifetimes that increase with increasingly native conditions (Figs. 1, 3 and 4). Examples are shown in Fig. 3(b–d). Once one of these structures is adopted under strongly native conditions ( $\epsilon/k_B T > 1.55$ ), it takes longer on average to reach the ground state if intrachain native contacts are more favorable

(Fig. 1). Folding trajectories under strongly native conditions are qualitatively different from that under milder conditions [Fig. 4(a-c)]. At the transition midpoint [Fig. 4(c)], interconversions between  $Q \approx 0.2$  and  $Q \approx 1.0$  are sudden and sharp. Relatively little time is spent at intermediate  $Q$  values. As  $\epsilon/k_B T$  increases, however, certain conformations with intermediate  $Q \approx 0.6-0.8$  are frequented more. Even under mildly native conditions, their impeding effects on folding kinetics is already apparent from the event in Fig. 4(b) depicting the chain bounces back to  $Q \approx 0.2$  after achieving  $Q \approx 0.8$ . But the lifetimes of these “intermediates” are brief compared to that of the open unfolded conformations. Hence folding remains approximately single-exponential [triangles in Fig. 2(b)]. However, when conditions become more strongly native [Fig. 4(a)], some folding trajectories are dominated by “intermediates,” leading to a significant reduction in average folding time. But even under these circumstances it is still possible to fold quickly [Fig. 4(a), inset]. Consistent with Fig. 2b (circles), this separation of time scales means that folding is no longer single-exponential.

In contrast to a previous report that no “entangled misfolded state” was observed during the folding of this particular G $\bar{o}$  model [14], Fig. 3(b) exhibits an overall nonnative topology. For Fig. 3(c), the left side of the conformation is native, but the right side is substantially nonnative. Hence these conformations are kinetic traps in that they cannot reach the ground state without first open up somewhat by breaking some existing favorable contacts. Notwithstanding possible artifacts of lattice models [Fig. 3(d)], this basic physical requirement rationalizes folding-arm chevron rollover because favorable contacts contributing to the meta-stability of these traps are increasing difficult to break with stronger  $-\epsilon/k_B T$ .

This prediction appears to be robust over a range of lattice and continuum coarse-grained models [Fig. 4(d-e)] that exhibit chevron rollovers. Fig. 4(d) shows that folding of a recent lattice model with residue-based as well as native-centric interactions are similar to that in Fig. 4(b). Fig. 4(e) shows that folding of a continuum  $C_\alpha$  model under mildly and strongly [inset in (e)] native conditions are very much similar, respectively, to the corresponding lattice results in Fig. 4(b) and (a). The trajectories in Fig. 4(f) from a continuum model [17] with desolvation barriers [26] also show that intermediate  $Q$  values are more prominent

during the folding process when conditions are more strongly native [inset in (f)].

A maximum (or “optimal”) folding rate similar to those in Fig. 1 have been observed in many models (e.g., [19,20,21,23,25]) since it was first noted in HP model simulations more than a decade ago [27]. This feature arises from a competition between a stronger driving force for folding and the onset of glassy dynamics under strongly native conditions (see note added in proof of [20]). However, until recently [11,17], the connection between this theoretical phenomenon and chevron rollover has not been recognized. Perhaps this is because the maximum folding rate often occurs near the transition midpoint for less cooperative models, and hence its relationship with chevron plots is less obvious. In contrast, the models studied here possess proteinlike thermodynamic cooperativity [16]. Several basic principles now emerge: (i) Rollovers can arise from kinetic trapping [6,9,20]; but folding relaxation remains approximately single exponential when trapping effects are mild [Fig. 2(b)]. (ii) We have rationalized rollovers phenomenologically by front factors that depend on  $\Delta G_u$  [11,17]. Physically, this dependence is likely caused by trapping and unfolding (barrier recrossing) from transiently populated compact non-ground-state conformations (Fig. 4). These predictions are testable by experiments. (iii) The chevron rollovers in the  $G\bar{o}$  models presented suggest strongly that, contrary to expectation,  $G\bar{o}$ -like pairwise additive interactions are insufficient [17] to capture the remarkable kinetics of small single-domain proteins [1]; further research is necessary to ascertain the physical origin of their simple two-state cooperativity.

The authors thank Walid Houry for a very helpful discussion. This work was supported in part by Canadian Institute of Health Research grant MOP-15323.

## REFERENCES

- [1] A. R. Fersht, *Curr. Opin. Struct. Biol.* **7**, 3 (1997); D. Baker, *Nature* **405**, 39 (2000).
- [2] S. E. Jackson and A. R. Fersht, *Biochemistry* **30**, 10428 (1991).
- [3] C. R. Matthews, *Methods Enzymol.* **154**, 498 (1987).
- [4] A. Matouschek et al., *Nature* **346**, 440 (1990).
- [5] W. A. Houry, D. M. Rothwarf and H. A. Scheraga, *Nature Struct. Biol.* **2**, 495 (1995).
- [6] T. Kiefhaber, *Proc. Natl. Acad. Sci. USA* **92**, 9029 (1995).
- [7] M. Silow and M. Oliveberg, *Proc. Natl. Acad. Sci. USA* **94**, 6084 (1997); D. E. Otzen et al., *Biochemistry* **38**, 6499 (1999).
- [8] R.-A. Chu and Y. Bai, *J. Mol. Biol.* **315**, 759 (2002).
- [9] R. Li, J. L. Battiste and C. Woodward, *Biochemistry* **41**, 2246 (2002).
- [10] R. L. Baldwin, *Fold. Des.* **1**, R1 (1996).
- [11] H. Kaya and H. S. Chan, *J. Mol. Biol.* **315**, 899 (2002).
- [12] K. W. Plaxco *et al.*, *Biochemistry* **39**, 11177 (2000).
- [13] C. Micheletti *et al.*, *Phys. Rev. Lett.* **82**, 3372 (1999).
- [14] V. S. Pande and D. S. Rokhsar, *Proc. Natl. Acad. Sci. USA* **96**, 1273 (1999).
- [15] C. Clementi, H. Nymeyer and J. N. Onuchic, *J. Mol. Biol.* **298**, 937 (2000).
- [16] H. Kaya and H. S. Chan, *Proteins Struct. Funct. Genet.* **40**, 637 (2000); *Phys. Rev. Lett.* **85**, 4823 (2000).
- [17] H. Kaya and H. S. Chan, *J. Mol. Biol.* **326**, 911 (2003).
- [18] E. Shakhnovich and A. R. Fersht, *Curr. Opin. Struct. Biol.* **8**, 65 (1998); V. S. Pande *et al.*, *Curr. Opin. Struct. Biol.* **8**, 68 (1998); R. L. Baldwin and G. D. Rose, *Trends*

- Biochem. Sci. **24**, 77 (1999); S. W. Englander, Annu. Rev. Biophys. Biomol. Struct. **29**, 213 (2000).
- [19] J. D. Bryngelson *et al.*, Proteins Struct. Funct. Genet. **21**, 167 (1995); K. A. Dill *et al.*, Protein Sci. **4**, 561 (1995); D. Thirumalai and S. A. Woodson, Acc. Chem. Res. **29**, 433 (1996).
- [20] H. S. Chan and K. A. Dill, Proteins: Struct. Funct. Genet. **30**, 2 (1998).
- [21] M. S. Li and M. Cieplak, Eur. Phys. J. B **14**, 787 (2000).
- [22] J. N. Onuchic *et al.*, Fold. Des. **1**, 441 (1996).
- [23] N. D. Socci, J. N. Onuchic and P. G. Wolynes, J. Chem. Phys. **104**, 5860 (1996).
- [24] J. Sabelko, J. Ervin and M. Gruebele, Proc. Natl. Acad. Sci. USA **96**, 6031 (1999).
- [25] V. I. Abkevich, A. M. Gutin and E. I. Shakhnovich, J. Chem. Phys. **101**, 6052 (1994).
- [26] M. S. Cheung, A. E. García and J. N. Onuchic, Proc. Natl. Acad. Sci. USA **99**, 685 (2002).
- [27] R. Miller *et al.*, J. Chem. Phys. **96**, 768 (1992).



**Fig. 1** MFPT is mean first passage time,  $k_B T$  is Boltzmann constant times absolute temperature. Circles are for the 48mer  $G\bar{o}$  model [14]. Squares are data from a model with the same ground-state conformation and attractive energy  $\epsilon$  for each native contact but with an additional repulsive energy  $-\epsilon$  for each nonnative contact (as in the HP+ model [20] and Ref. [21]). Folding (open symbols) starts from a random self-avoiding walk, first passage is achieved when  $Q = 1$ . Unfolding (filled symbols) starts from the  $Q = 1$  ground state, first passage is achieved when  $Q \leq 6/57$  because the free energy minimum of the denatured states is at  $Q \approx 6/57$ . Solid dashed curves are mere guide for the eye. The vertical dotted lines mark the two model's thermodynamic transition midpoints. The two pairs of V-shape dotted lines are hypothetical simple two-state chevron plots [11] based upon  $\Delta G_u$  between  $Q = 1$  and  $Q \leq 6/57$  obtained by histogram techniques from sampling around the transition midpoint. The triangles, asterisks, and diamonds are  $-\ln(\text{MFPT})$  values for  $G\bar{o}$ -model folding initiated (at  $t = 0$ ) respectively from the compact conformations (b), (c), and (d) in Fig. 3. Arrows indicate the  $\epsilon/k_B T$  values considered in Fig. 2.

**Fig. 2** (a) Free energy profiles for the  $G\bar{o}$  model at the  $\epsilon/k_B T$  values indicated (c.f. Fig. 1).  $P(Q)$  is Boltzmann population distribution over  $Q$ . [Note that  $P(Q) = 0$  for  $Q = 55/57$  and  $56/57$ .] (b)  $P(t)\Delta t$  is the fraction of folding trajectories with  $t - \Delta t/2 < \text{first passage time} \leq t + \Delta t/2$  [17], plotted in different horizontal scales for different  $\epsilon/k_B T$ s [symbols as in (a)] to enhance clarity. For  $\epsilon/k_B T = -1.82, -1.61, -1.47, \text{ and } -1.28$  respectively, 2,500, 2,030, 3,500, and 1,100 trajectories are analyzed using  $\Delta t/10^6 = 30, 1.8, 1.6, \text{ and } 30$ ; the  $\ln[P(t)\Delta t]$  shown are for  $t$  values equal to 1, 1/10, 1/20, and 1/2 of that given by the horizontal axis. Solid and dashed lines are linear fits for  $\epsilon/k_B T = -1.47$  and  $-1.28$ .

**Fig. 3** (a) Ground state of the  $G\bar{o}$  model. (b–d) Transiently trapped conformations under strongly native conditions (c.f. Fig. 1), with  $Q = 39/57, 41/57$  and  $53/57$  respectively. The dotted, dashed, dotted-dashed lines and filled circles are used to identify monomers (in all four conformations) that belong to three of the straight edges and the core positions in the

ground-state conformation (a). The conformation in (d) may reach the ground state by a simple hinge motion of the dotted-dashed edge. However, since such a move is not available in the model [14], the chain now must first partially open up before it can access the ground state. The trapping effect of (d) is minor compared to that of (b) and (c) (see Fig. 1).

**Fig. 4** (a–c) Folding trajectories of the 48mer  $G\bar{o}$  model at  $\epsilon/k_B T = -1.82$  (a),  $-1.47$  (b), and  $-1.28$  (c). The insets in (a, b) each shows a faster folding trajectories at the same given  $\epsilon/k_B T$ . (d–f) Typical folding trajectories in other models for comparison: (d) is from a 55mer lattice model under mildly native conditions ( $\epsilon/k_B T = -1.75$ ) [11]. (e, f) are from the continuum NCS1 without-solvation (e) and with-solvation (f) Langevin dynamics models at  $T = 0.82$  for CI2 [17] with  $\epsilon = 0.88$  (e) and  $1.1$  (f). The insets in (e, f) show trajectories at the same  $T$  but under more strongly native conditions at  $\epsilon = 1.0$  (e) and  $1.5$  (f).

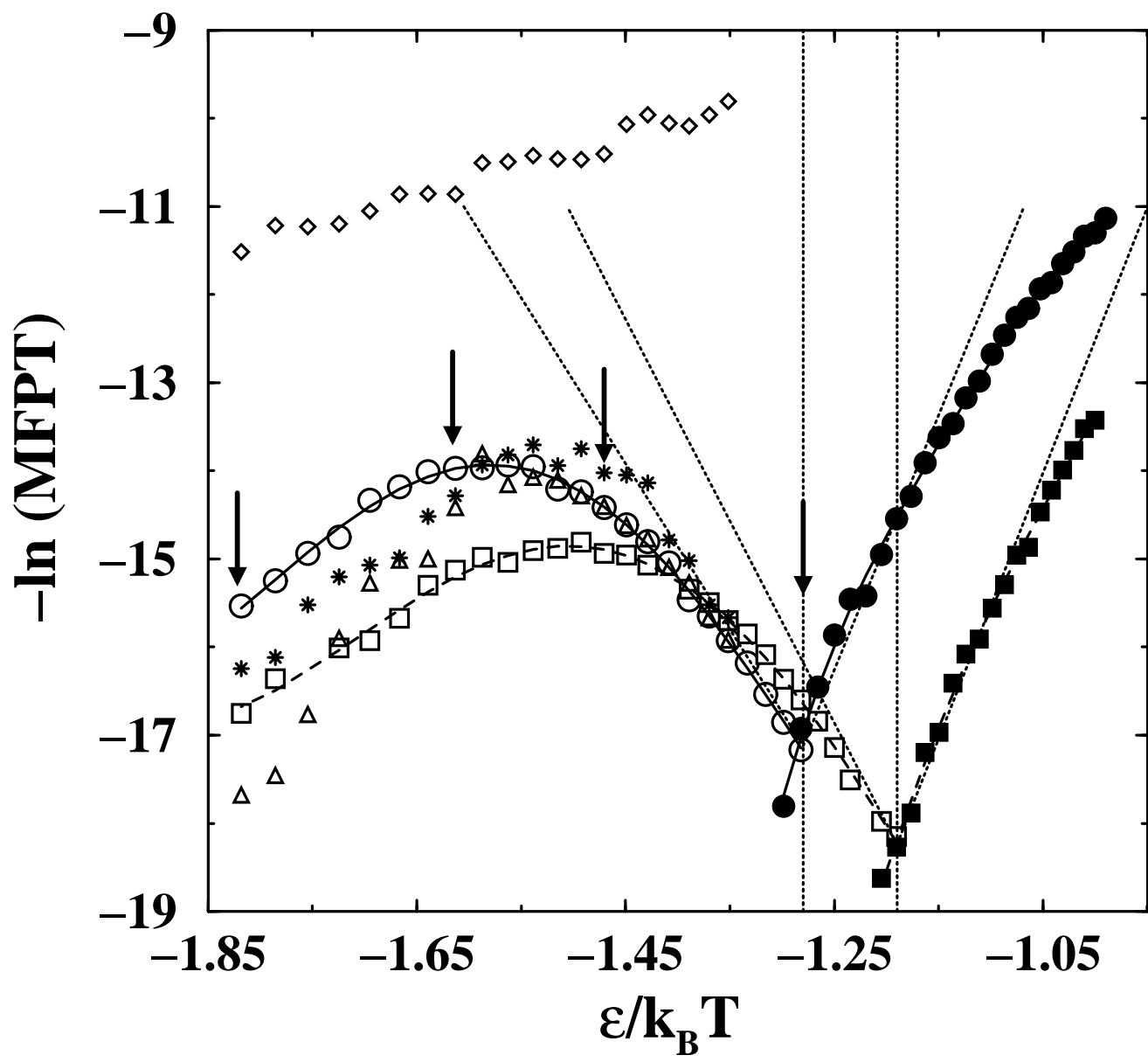


Fig.1

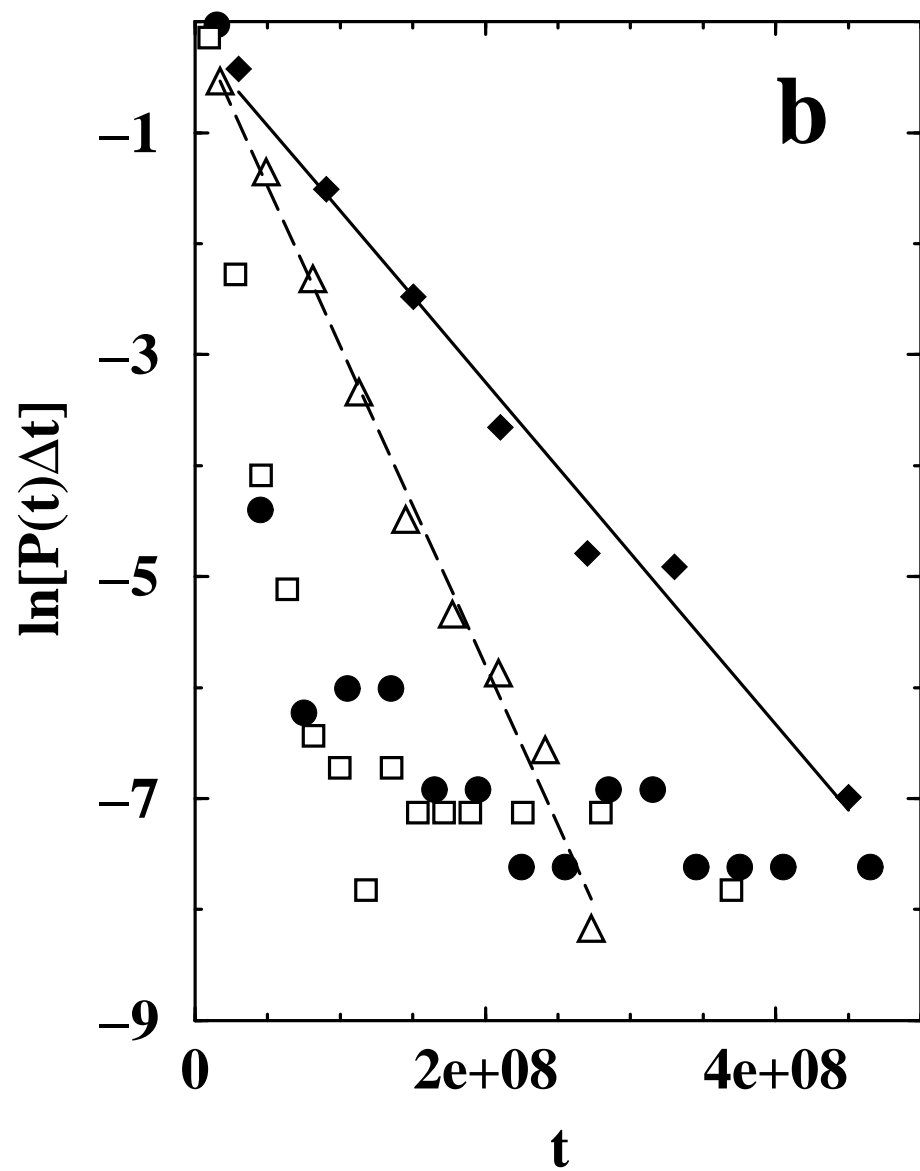
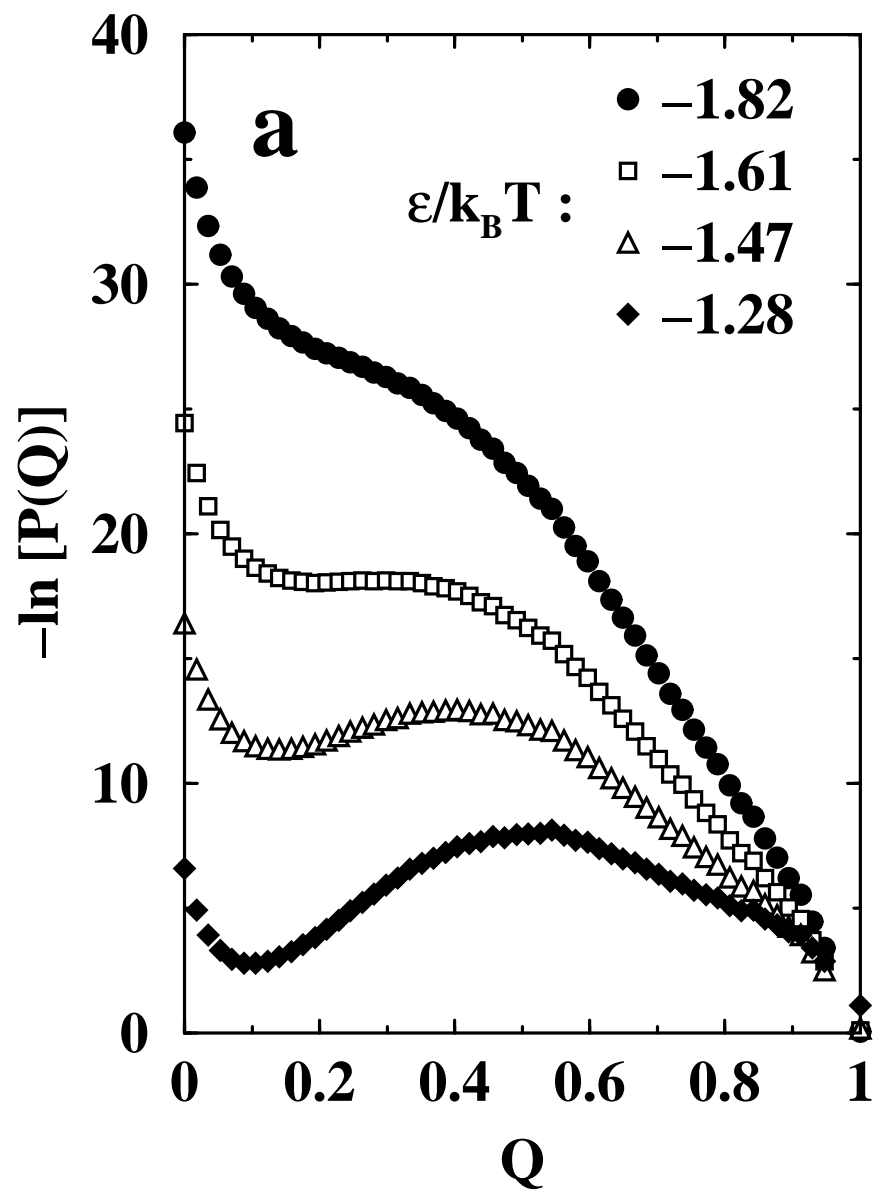
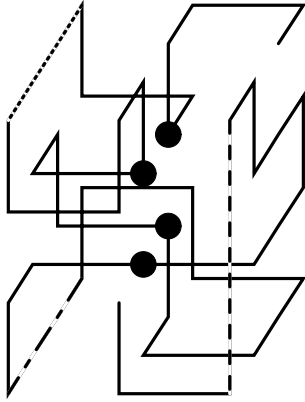
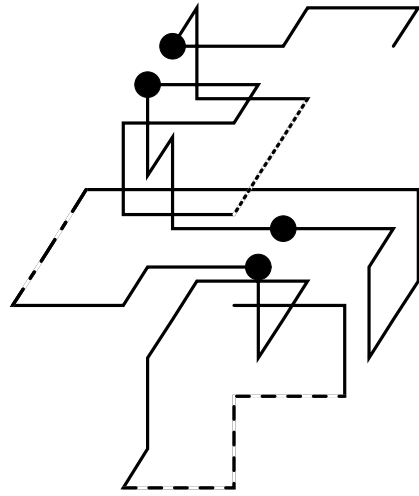


Fig.2

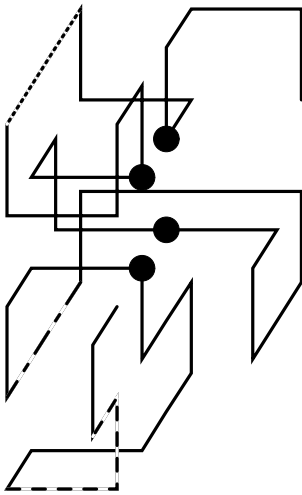
**a**



**b**



**c**



**d**

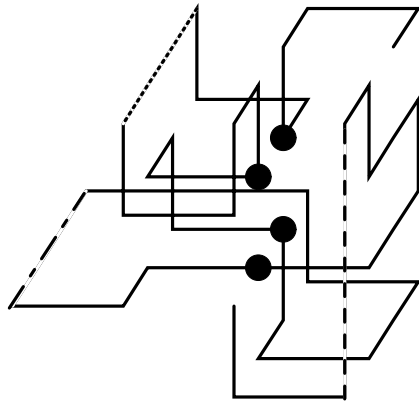


Fig.3

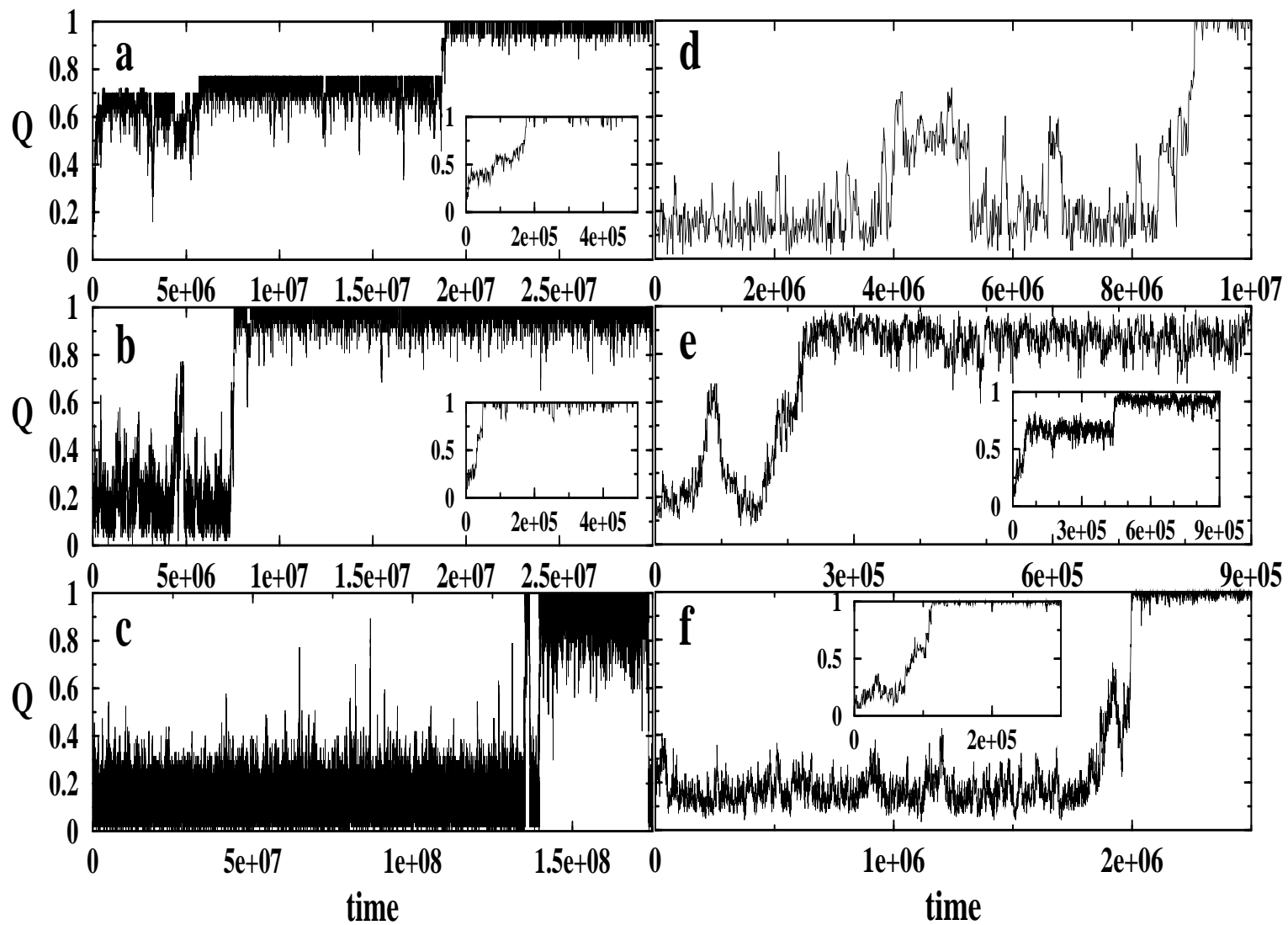


Fig.4